Analytica Chimica Acta 1162 (2021) 338503

Contents lists available at ScienceDirect

Analytica Chimica Acta

journal homepage: www.elsevier.com/locate/aca

Dark-field microscopic real-time monitoring the growth of Au on Cu_2O nanocubes for ultra-sensitive glucose detection

Yang Zhao, Wei Zhao**, Hong-Yuan Chen, Jing-Juan Xu*

State Key Laboratory of Analytical Chemistry for Life Science, School of Chemistry and Chemical Engineering, Nanjing University, Nanjing, 210023, China

HIGHLIGHTS

- The scattering imaging strategy is used to in situ monitor the growth of Au on Cu_2O surface.
- The Cu_2O/Au nanostructures could be precisely controlled via the scattering signal.
- The prepared Cu_2O/Au nanocomposite has a higher electrocatalytic activity toward Glucose.
- The paper provides a convenient approach in controllable synthesis of plasmonic electrocatalysts in biosensing.

GRAPHICAL ABSTRACT

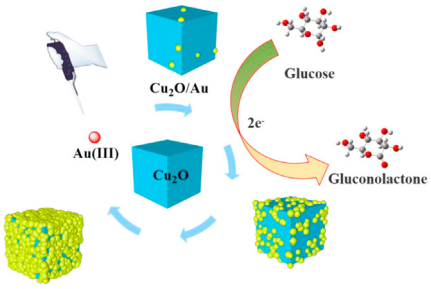

ARTICLE INFO

Article history:
Received 17 March 2021
Received in revised form
30 March 2021
Accepted 5 April 2021
Available online 12 April 2021

Keywords:
DFM
LSPR
Cu_2O/Au nanocubes
Nonenzyme
Glucose sensor

ABSTRACT

Nanoparticle plasmon scattering **can provide real-time imaging information on the formation process of noble metal-based nanomaterials.** Due to the synergistic effect of the interface between metal and oxide supporting pores, metal nanoparticles (NPs), especially Au NPs, generally exhibit higher catalytic activity on oxide carriers than single-component NPs. Here, we use the dark field scattering microscope to in situ monitor the growth of Au on Cu_2O surface by oxidation-reduction reactions and the nanostructures could be precisely controlled via the scattering signal. The prepared Cu_2O/Au nanocomposite has a higher electrocatalytic activity toward Glucose. When being used as a potential biosensor for nonenzyme glucose detection, excellent performance, such as high sensitivity with a detection limit of 4 μM, high selectivity and outstanding stability, was obtained. The scattering imaging strategy is a convenient and universal approach in controllable synthesis of plasmonic heterostructures, and leads to the improvement of electrocatalysts in biosensing.

1. Introduction

Dark field microscopy (DFM) is widely used in biological and material research, such as biosensor [1], material synthesis [2], disease diagnosis [3], and unlabeled living tissue imaging [4]. The local surface plasmon resonance (LSPR) of noble metal nanoparticles is affected by the particle composition, shape, size and surrounding media [5]. When the size, shape and composition of nanomaterials change, the specific scattering peak will also be red shifted or blue shifted. The emergence of dark field scattering microscope enables us to observe the dynamic changes of LSPR of single noble metal nanoparticles, so as to monitor the growth process of noble metal nanoparticles in real time. For example, Huang and coworkers reported the application of dark field

* Corresponding author.
** Corresponding author.
E-mail addresses: weizhao@nju.edu.cn (W. Zhao), xujj@nju.edu.cn (J.-J. Xu).

https://doi.org/10.1016/j.aca.2021.338503
0003-2670/

scattering microscope in real-time monitoring of single Ag@Hg in situ growth of nanoalloys [2].

As we all know, cuprous oxide (Cu_2O) has been widely studied because of its potential applications in catalysis [6], biocides [7], gas sensors [8], solar energy photovoltaics [9], lithium-ion batteries [10,11] and so on. A considerable number of literatures reported the preparation of Cu_2O crystals with different morphologies, such as nanowires, spheres, cubes, octahedrons, cubic octahedrons, truncated octahedrons, dodecahedrons, 26 faceted polyhedrons, 50 faceted polyhedrons, and so on [12,13]. Among them, cubic and octahedral Cu_2O crystals are the most important, because more complex structures can be derived from them, and their well-defined faces provide a unique opportunity to examine their face dependent properties. However, due to the high electron hole recombination rate and wide size distribution of pure Cu_2O, its catalytic performance is far from ideal. The introduction of Au particles can overcome these shortcomings. At the same time, the synergistic effect of noble metal nanoparticles (NPs) and oxide support pore interface makes NPs/metal oxide show higher catalytic activity than single component NPs. This is because the electronic structures of metal and oxide carriers are changed by the electron transfer at the interface, which results in oxygen cavitation on the interface oxide carrier and thus becomes the active site for oxygen absorption and activation [14–17].

In recent years, the number of patients with diabetes has been increasing year by year, and detecting the glucose content in blood is the key to prevent diabetes [18–22]. Therefore, it is extremely urgent to develop a glucose sensor with high sensitivity and high selectivity. At present, a variety of glucose sensors have been used to monitor the blood glucose content, such as electrochemical [23], fluorescent [24], optical [25] and transdermal [26]. Among these methods, electrochemical glucose sensor has attracted extensive attention due to its small size, weak background signal, high sensitivity, good selectivity and fast response time [27,28]. The traditional electrochemical detection methods of glucose mostly involve the use of glucose oxidase (GOD), which can quickly and accurately identify glucose molecules by catalyzing the oxidation of glucose to glucolactone [29,30]. As the sensors related to enzymes are very sensitive to temperature, pH and humidity, which seriously hinders the further development of enzyme sensors, non-enzymatic glucose sensors based on various electrocatalysts for the electrocatalytic oxidation of glucose have attracted more and more attention as a substitute [31]. In order to develop an efficient, highly sensitive enzyme-free glucose sensor, a good catalytic material is needed.

In this work, we reported the application of dark field scattering microscope in real-time monitoring of the growth of single Cu_2O/Au for enzyme-free glucose detection, as shown in Fig. 1. Firstly, Cu_2O nanocubes were synthesized with a solution chemistry route, and then the growth process of Cu_2O/Au nanocubes were monitored by LSPR of noble metals under dark field microscope (DFM).

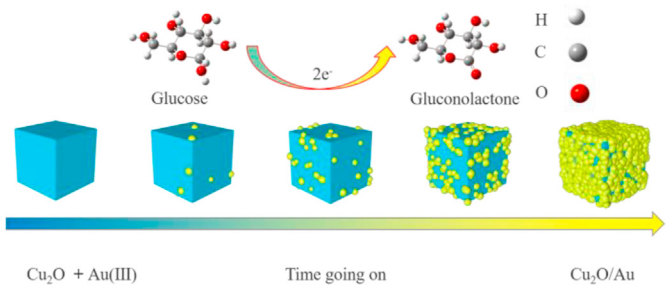

Fig. 1. Schematic illustration of Cu_2O/Au NPs for non-enzymatic glucose detection.

Finally, the nanomaterials with high electrochemical activity were applied to the highly sensitive detection of glucose. Due to the synergistic effect of the interface between metal and oxide supporting pores, metal nanoparticles (NPs), especially Au NPs, generally exhibit higher catalytic activity on oxide carriers than single-component NPs. This results in Cu_2O/Au having a stronger ability to catalyze glucose than Cu_2O. The sensor presents a satisfactory sensitivity (2891 μA mM^{-1} cm^{-2}) and comparatively low detection limit of 4 μM. This work provides a simple strategy for controllable synthesis of plasmonic heterostructures, and leads to the improvement of electrocatalysts in biosensing.

2. Experimental section

2.1. Reagents

Copper chloride ($Cu(Cl)_2 \cdot 2H_2O$) was purchased from Shanghai Sinpeuo Fine Chemical Co., Ltd. Sodium hydroxide (NaOH), urea, uric acid (UA) and sodium chloride (NaCl) were purchased from Aladdin Chemical Reagent (Shanghai, China). Acetic acid, poly (ethylene glycol) (PEG, mw = 10,000), chitosan, fructose and lactose were obtained from Sinopharm Chemical Reagent (Shanghai, China). Ascorbic acid (AA) was obtained from Sigma-Aldrich. All chemicals were of analytical grade and used without further purification. The deionized water (18.25 MΩ cm) used in all of the preparation was from a MilliQ Academic water purification system.

2.2. Synthesis of Cu_2O nanomaterials

In the experiment, all glass instruments were soaked in aqua regia and dried in advance. The preparation of Cu_2O nanocrystals is reported in the previous literature [32]. In briefly, 10 g of PEG and 3.4 mg of $Cu(Cl)_2$ were first dissolved in 200 mL aqueous solution. After stirring for 20 min, PEG was completely dissolved, and then 1 mL of NaOH solution (6.0 M) was dropwise added. The solution immediately changed to light blue color, which indicated the formation of $Cu(OH)_2$ nanoparticles. After 10 min, 4 mL of AA solution (1 M) was dropwise added to the solution. Then leave it at room temperature for half an hour. Finally, the obtained precipitates were washed with ultrapure water and ethanol several times and then stored in ethanol solution.

2.3. Dark-field scattering microscopic monitoring of the growth of Cu_2O/Au nanocubes

We use a DFM equipped with a 60 × objective lens (NA = 0.7), 100 W halogen lamp as the white light source and a dark-field condenser (0.8 < NA < 0.92) for imaging. We attached the Cu_2O nanocrystals to a positively charged glass plate by electrostatic attraction with a poly (dimethyl siloxane) (PDMS) reservoir (1 cm diameter, ~200 μL total volume). The sample was prepared by dropping 200 μL of solution containing the Cu_2O into the PDMS reservoir and kept for 2 min. It was washed three times with 200 μL of secondary water to remove unadsorbed nanoparticles, and dried with nitrogen. Then, 200 μL of filtered water was added to the groove for dark-field imaging. After that, 10 μL of $NaAuCl_4$(0.1 mM) was added to the solution, which was reduced in situ to form Cu_2O/Au under a true-color digital camera (Olympus DP80, Japan). Cu_2O/Au NPs with different Au contents were obtained by controlling the reaction time.

2.4. Fabrication of the glucose sensor and measurements

All electrochemical measurements were carried out in a three-electrode system using CHI 760e electrochemical workstation

(Shanghai CH Instruments, China) at room temperature. A glassy carbon electrode (GCE) with a diameter of 3 mm, a Pt electrode wire and standard calomel electrode (SCE) were used as the working electrode, counter electrode and reference electrode, respectively. Before electrochemical experiments, the GCE was polished with alumina suspension and then ultrasonically cleaned in ethanol and deionized water. In order to prevent the nanomaterials falling off the electrodes during glucose detection, 10 μL of chitosan solution (0.001 g chitosan dissolved in 10 mL 0.1% acetic acid) was added to 40 μL of Cu_2O/Au NPs solution, then 10 μL of the mixed solution was taken and coated on the electrode to form a stable film. Electrochemical activity was assessed by current–time response with a rotation at a scan rate of 100 mV s^{-1} at 0.6 V in 0.1 M NaOH solution.

2.5. Characterization of materials

Transmission electron microscopy (TEM) images were obtained on a JEM-2800 (JEOL, Japan) instrument. The X-ray photoelectron spectrum (XPS) was obtained from a PHI 5000 VersaProbe (U1VAC-PHI Co., Japan). X-ray diffraction (XRD) spectra were characterized using a powder X-ray diffractometer (ARL Co., Switzerland) with Cu Kα radiation.

3. Results and discussion

3.1. Characterization of Cu_2O and Cu_2O/Au nanomaterials

Firstly, the electrode materials were characterized by TEM, as shown in Fig. S1. As can be seen in Fig. S1 A and B, the TEM images reveal monodispersed Cu_2O nanocubes with average side length of 50 nm and the lattice fringe spacings of 0.246 nm, which was close to the spacing of the (111) plane of crystalline Cu_2O. In order to determine the distribution of elements on the Cu_2O NPs, the EDS elemental mapping was carried out, as shown in Fig. S1 C. The atomic percentages of Cu and O are 66.18%, and 33.82%, respectively.

Galvanic replacement reaction (GRR) between Cu_2O and $NaAuCl_4$ follows the reaction:

$$3Cu2O + 2AuCl4 - + 3H2O = 6Cu2 + + 2Au + 8Cl - + 6OH- \quad (1)$$

The Cu_2O/Au in different time periods were characterized by TEM, as shown in Fig. 2A. After the formation of Cu_2O/Au NPs, it was found that the surface of Cu_2O nanocrystals became rough and formed a lot of protrusions, indicating the formation of Au. As can be seen from Fig. 2A, in the first few seconds of the reaction, less gold was precipitated and distributed sporadically on the Cu_2O surface. With the prolongation of reaction time, more and more Au adhered to the surface of Cu_2O. However, when the reaction time is 450 s, Cu_2O/Au nanoparticles will not guarantee their integrity and become a pile of scattered gold nanoparticles, as shown in Fig. S2. Due to the strong LSPR characteristics of precious metals, the reduction process of Au (III) on Cu_2O can be observed in real time by LSPR scattering imaging. Next, the growth process of Au on the same Cu_2O nanocube was monitored in DFM. As shown in Fig. 2B and C, individual Cu_2O NP was observed as blue spot under DFM with the scattering spectra at 485 nm. In the presence of Au (III), the scattering spectrum of the nanoparticles gradually redshifted to 666 nm and showed orange spots in the dark field microscope. When the reaction time exceeds 350s, the scattering spectrum peak of nanoparticles would not change, only the peak intensity shows a slight increase.

Since the color of nanocrystals changed significantly under DFM, ImageJ was used to conduct color analysis of dark field images and extracted the red/green (R/G) value of each point. It can be seen from Fig. 2 D that the R/G value of the nanocube presents a linear change before 300 s, which is mainly determined by the quantitative relationship of the redox reaction. We further used energy dispersive spectrometer (EDS) to analyze the ratio of the atomic composition, as shown in Fig. S3. As the reaction time increases, the content of Au gradually increases. When the reaction time is 350s, the ratio of Cu to Au is 24:1. Thus, we can accurately control the growth of Au NPs on Cu_2O nanocrystals through LSPR scattering variation.

The crystal structures of Cu_2O/Au were characterized by High resolution electron microscopic (HRTEM), X-ray diffractometer

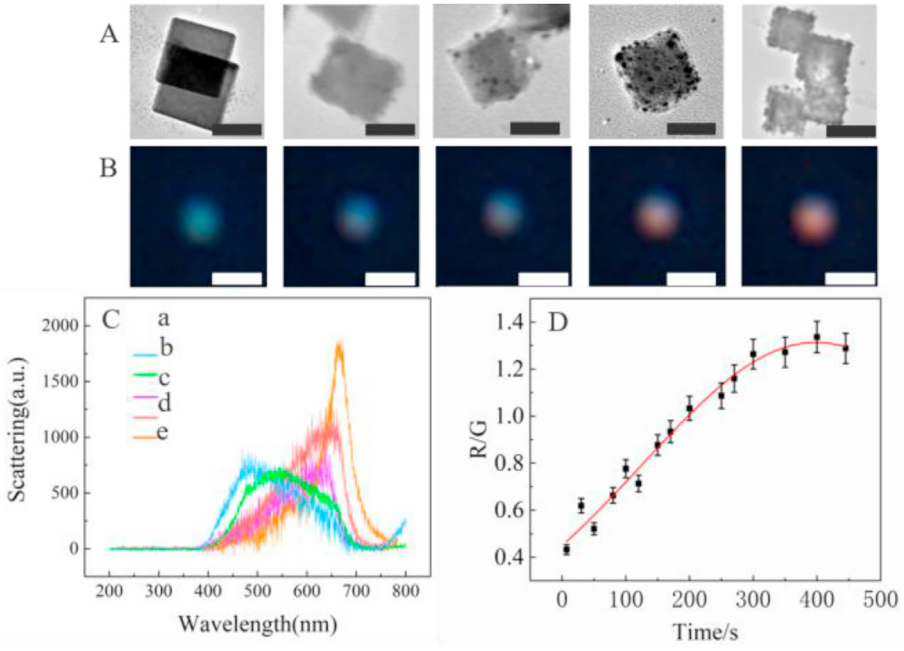

Fig. 2. (A) Time-dependent TEM images of Cu_2O/Au (0s, 7s, 120s, 300s, 350s, scale bar: 50 nm); (B) Time -dependent DFM images (scale bar: 10 μm) and (C) corresponding spectra of Cu_2O and Cu_2O/Au NPs. (D) R/G value trace of nanoparticles with time elapsing.

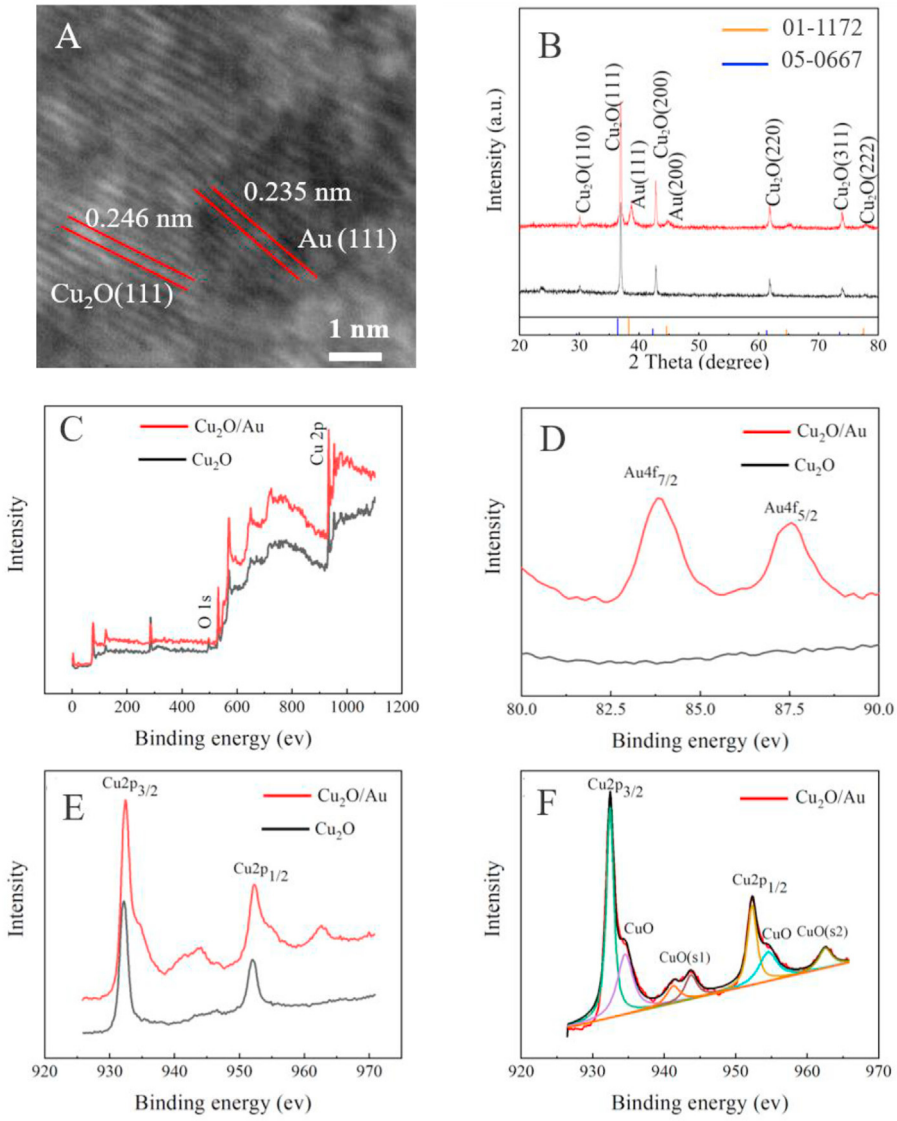

Fig. 3. (A) HRTEM image of Cu_2O/Au NPs, (B) XRD pattern of Cu_2O (a) and Cu_2O/Au(b), (C–F) XPS survey spectra of Cu_2O and Cu_2O/Au.

(XRD) and X-ray photoelectron spectroscopy (XPS). Cu_2O/Au with a reaction time of 300s was used as the experimental sample. Fig. 3 A shows a typical HRTEM image of the sample with the spacings of lattice fringes of 0.246 nm (Cu_2O,111) and 0.235 nm (Au,111). As shown in Fig. 3B, the XRD pattern of the sample presents strong Cu_2O (JCPDS: no. 05–0667) diffraction peaks ((110), (111), (200), (220), (311) and (222) facets) as well as Au peaks (111 and 200 facets), indicating the formation of Au NPs on Cu_2O nanocubes. In general, Fig. 3C–F are the XPS spectra of Cu2O and the Cu_2O/Au sample. Peaks such as Cu 2p and O 1s reflect the presence of Cu_2O. As shown in Fig. 3D, the Au 4f peak of Cu_2O/Au can be observed obviously by enlarging the XPS curve of Cu_2O/Au. There were two prominent peaks at 87.7 and 83.9 eV, which correspond well to Au $4f_{7/2}$ and Au $4f_{5/2}$ signals. Moreover, Fig. 3E reveals the high-resolution Cu 2p spectra of the Cu_2O and Cu_2O/Au, clearly indicating that Cu 2p1/2 and Cu 2p3/2 have strong signals of Cu_2O at 952.37 eV and 932.51 eV, respectively. While the weak signals at 934.57, 944.03, 954.95, and 963.28 eV are accredited to the CuO crystal phase due to oxidation of a small amount of Cu_2O, as shown in Fig. 3F.

3.2. Feasibility characterization

We then characterized the electrocatalytic activity of the materials by cyclic voltammetry (CV) and electrochemical impedance spectroscopy (EIS). We studied the response of electrode materials to glucose by CV in 0.1 M NaOH at scan rate of 100 mV s^{-1}. It can be seen from Fig. 4A that there is no change in the CV curve for the bare electrode with or without glucose. From Fig. 4B and C, we can see an obvious oxidation peak at about 0.42 V, which indicates that glucose could be electrooxidized on Cu_2O nanocubes and Cu_2O/Au nanocomposites modified electrode surfaces. Moreover, the catalytic activity of Cu_2O/Au for glucose is obviously better than that of Cu_2O, which is about two times of that of Cu_2O. Here we used 5 nm Au NPs (Fig. S4 and Fig. 4D) as a control, and proved that the improvement of glucose catalytic performance was not the catalysis of Au NPs itself, but the result of the synergistic effect of Au NPs on Cu_2O NPs. As shown in Fig. S5, the diameter of the semicircle portion in the EIS spectrum decrease in order: Cu_2O > bare GCE > Cu_2O/Au. The semicircle portion at higher frequencies is due to the electron transfer limited process and the linear portion at

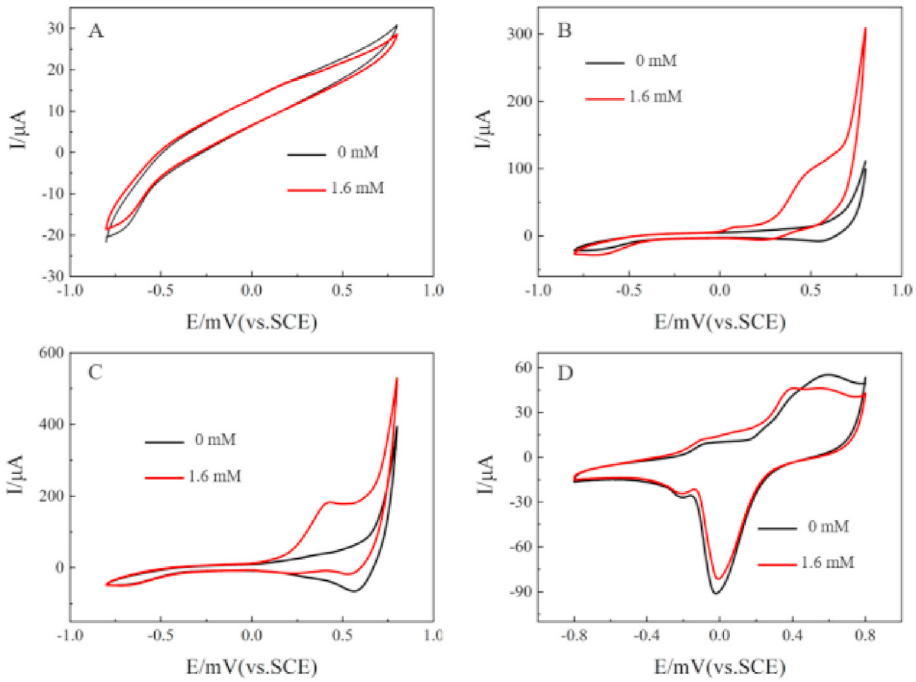

Fig. 4. CV curves of bare GCE (A), Cu_2O (B), Cu_2O/Au (C) and Au NPs (D) in 0.1 M NaOH with or without 1.6 mM glucose at scan rate of 100 mV s^{-1}.

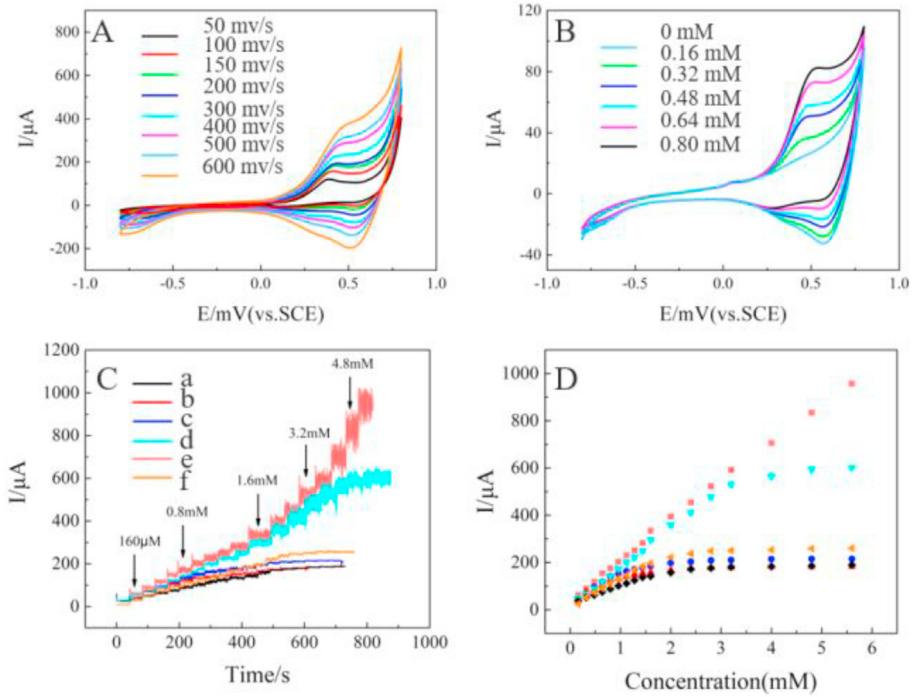

Fig. 5. (A) CV curves of the Cu_2O/Au electrode in 0.1 M NaOH solution containing 1.6 mM glucose at various scan rates. (B) CV curves of the Cu_2O/Au array electrode in 0.1 M NaOH solution containing different concentrations of glucose (from 0 to 0.8 mM) at a scan rate of 20 mV s-1. (C) Amperometric response curve of Cu_2O/Au modified electrode obtained in different reaction time (a:0s, b:7s, c:120s, d: 300s, e: 350s, f: 450s) after successive addition of glucose at detection potential of 0.6 V in 0.1 M NaOH. (D) The corresponding calibration curve from C.

lower frequencies is resulted from a diffusion limited process [33]. The diameter of the semicircle portion in the EIS spectrum can be quantified using the electron transfer resistance [34]. Among them, Cu_2O/Au has the best ability to transfer electrons.

3.3. Highly sensitive glucose detection

Furthermore, CV curves of Cu_2O/Au electrode in 0.1 m NaOH solution containing 1.6 mM glucose were studied at different scanning rates, as shown in Fig. 5A. The results shown that the oxidation peak current of glucose changed linearly (Fig. S6), which

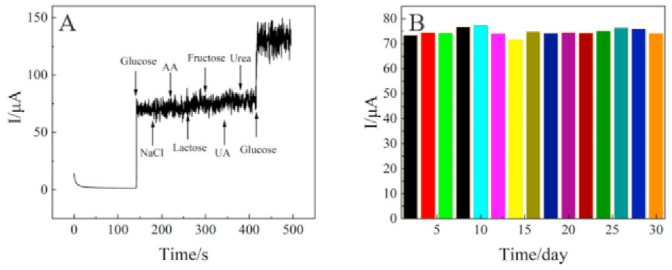

Fig. 6. (A) Amperometric response curve of Cu_2O/Au after successive addition of 0.40 mM glucose, 0.40 mM NaCl, 0.01 mM AA, 0.01 mM lactose, 0.01 mM fructose, 0.01 mM UA, 0.01 mM urea and 0.40 mM glucose in 0.1 M NaOH solution at 0.6 V. (B) Long-term stability of the Cu_2O/Au.

revealed that the electrochemical kinetics is governed by the adsorption of glucose on the surface of the electrodes. Fig. 5B showed the CV results of Cu_2O/Au at different glucose concentrations (from 0 to 0.8 mM) in 0.1 M NaOH aqueous solution. With the gradual addition of glucose, the anodic current increased significantly, indicating that Cu_2O/Au had good catalytic performance for glucose oxidation.

In order to obtain better current response signal, the detection potential was optimized. As can be seen from Fig. S7, the current signal generally shows an upward trend in the range of 0.4–0.7 V, which was because the higher the voltage, the faster the reaction rate. When the potential exceeds 0.6 V, the current change is not great, but the noise signal becomes more serious. Therefore, we applied a detection potential of 0.6 V for glucose sensing. We studied the sensitivity, selectivity and response time of glucose sensor by means of amperometric analysis. Current responses with the continuous addition of glucose (0.16–5.6 mM) in constantly stirred NaOH solutions were recorded at Cu_2O and Cu_2O/Au obtained in different reaction times, as shown in Fig. 5C. It can be seen that when the reaction time was less than 350 s, the catalytic performance of the Cu_2O/Au material to glucose enhanced with the increase of reaction time, that is, the increase of Au content. When the reaction time more than 350s, such as 450s, the catalytic performance decreases due to the weakening of the synergistic effect between the Cu_2O and Au by the reduction and broken of Cu_2O nanocubes, as shown in Fig. S2. Fig. 5D records the corresponding calibration curve. The Cu_2O/Au electrodes showed fast response towards glucose concentration changes, and the sensing currents increased with glucose concentration. The glucose sensor obtained at reaction time of 350s showed a good linear relationship between the concentration range from 0.16 mM to 5.6 mM comprising an admirable linear correlation coefficient value ($R = 0.999$). As shown in Table S1, the sensor presents a satisfactory sensitivity (2891 μA mM^{-1} cm^{-2}) compared with other sensors and comparatively low detection limit of 4 μM. The sensitivity of the Cu_2O/Au is almost 2-fold greater than that of the Cu_2O (1476 μA mM^{-1} cm^{-2}). Furthermore, the limit of detection (4 μM, S/N = 3) in Cu_2O/Au is lower than that of only Cu_2O (16.67 μM, S/N = 3).

3.4. Selective and stability characterization

An excellent sensor, in addition to having good sensitivity, should also have specific detection of the target in many interfering species. Since the concentration of glucose in human blood is much higher than that of other interferents, we studied the current response of Cu_2O/Au in 0.1 M sodium hydroxide solution by continuously adding 0.16 mM glucose and 0.01 mM other interferents. Fig. 6A shows that after the addition of these common interfering substances including 0.01 mM NaCl, 0.01 mM AA, 0.01 mM lactose, 0.01 mM fructose, 0.01 mM UA and 0.01 mM urea, the current changes can be ignored, while the target analyte still gets a clear response signal. We verify the stability and reproducibility of the sensor. We can see that the current remains at 98% of its original value over a running time of 1500 s (Fig. S8). Finally, the long-term stability of the Cu_2O/Au was explored by recording the current response toward 0.16 mM glucose over 30 days, as shown in Fig. 6B. The amperometric response was not obviously changed after 30 days, suggesting excellent stability of Cu_2O/Au.

4. Conclusion

In conclusion, we used dark field scattering microscope real-time monitoring the growth of Au NPs on Cu_2O nanocubes to obtain Cu_2O/Au nanocomposite with high synergistic catalytic effect to glucose. The obtained glucose sensor showed a good linear relationship between the concentration range from 0.16 mM to 5.6 mM and presented a satisfactory sensitivity (2891 μA mM^{-1} cm^{-2}) and comparatively low detection limit of 4 μM. The overall results illustrate that the Cu_2O/Au presents brilliant prospects for glucose detection, especially for the analysis of extremely low concentrations of glucose. This work also provides a simple strategy for controllable synthesis of plasmonic heterostructures, and leads to the improvement of electrocatalysts in biosensing.

CRediT authorship contribution statement

Yang Zhao: Designing and conducting experiments, writing-original draft. Wei Zhao: Conceptualization and data analysis. Hong-Yuan Chen and Jing-Juan Xu: Conceptualization, writing-review & editing, project administration. All authors discussed the results and reviewed the manuscript.

Declaration of competing interest

The authors declare that they have no known competing financial interests or personal relationships that could have appeared to influence the work reported in this paper.

Acknowledgment

This work was supported by the National Natural Science Foundation of China (Grants 22034003, and 22074063) of China, and Fundamental Research Funds for the Central Universities.

Appendix A. Supplementary data

Supplementary data to this article can be found online at https://doi.org/10.1016/j.aca.2021.338503.

References

[1] Y. Choi, Y. Park, T. Kang, L.P. Lee, Selective and sensitive detection of metal ions by plasmonic resonance energy transfer-based nanospectroscopy, Nat. Nanotechnol. 4 (2009) 742–746.
[2] Y. Liu, C.Z. Huang, Real-time dark-field scattering microscopic monitoring of the in-situ growth of single Ag@Hg nanoalloys, ACS Nano 7 (2013) 11026–11034.
[3] K. Lee, Y. Cui, L.P. Lee, J. Irudayaraj, Quantitative imaging of single mRNA splice variants in living cells, Nat. Nanotechnol. 9 (2014) 474.
[4] L. Zhang, Y. Li, D.W. Li, C. Jing, X. Chen, M. Lv, Q. Huang, Y. Long, I. Willner, Single gold nanoparticles as real-time optical probes for the detection of NADH-dependent intracellular metabolic enzymatic pathways, Angew. Chem. 123 (2011) 6921–6924.
[5] M.B. Cortie, A.M. McDonagh, Synthesis and optical properties of hybrid and alloy plasmonic nanoparticles, Chem. Rev. 111 (2011) 3713–3735.
[6] M. Hara, T. Kondo, M. Komoda, S. Ikeda, J.N. Kondo, K. Domen, M. Hara,

K. Shinohara, A. Tanaka, Cu_2O as a photocatalyst for overall water splitting under visible light irradiation, chem, Commun. Now. 3 (1998) 357–358.
[7] H. Pang, F. Gao, Q. Lu, Morphology effect on antibacterial activity of cuprous oxide, chem, Commun. Now. 9 (2009) 1076–1078.
[8] M. Kevin, W. Ong, G. Lee, G. Ho, formation of hybrid structures: copper oxide nanocrystals templated on ultralong copper nanowires for open network sensing at room temperature, Nanotechnology 22 (2011) 235701.
[9] B. Rai, Cu_2O solar cells: a review, sol, Cells 25 (1988) 265–272.
[10] C. Huang, L. Zheng, M. Miyauchi, X. Qiu, A facile one-pot synthesis of Cu-Cu_2O concave cube hybrid architectures,, CrystEngComm 16 (2014) 4967–4972.
[11] P. Poizot, S. Laruelle, S. Grugeon, L. Dupont, J. Tarascon, Nano-sized transition-metal oxides as negative-electrode materials for lithium-ion batteries, Nature 407 (2000) 496–499.
[12] J.Y. Ho, M.H. Huang, Synthesis of submicrometer-sized Cu_2O crystals with morphological evolution from cubic to hexapod structures and their comparative photocatalytic activity, J. Phys. Chem. C 113 (2009) 14159–14164.
[13] Y. Zhang, B. Deng, T. . Zhang, D. Gao, A.-W. Xu, Shape effects of Cu_2O polyhedral microcrystals on photocatalytic activity, J. Phys. Chem. C 114 (2010) 5073–5079.
[14] Z.P. Liu, X.Q. Gong, J. Kohanoff, C. Sanchez, P. Hu, Catalytic role of metal oxides in gold-based catalysts: a first principles study of CO oxidation on TiO_2 supported Au,, Phys. Rev. Lett. 91 (2003) 266102.
[15] J.D. Grunwaldt, A. Baiker, Gold/Titania Interfaces, Their Role, In carbon monoxide oxidation, J. Phys. Chem. B 103, 1999, p. 1002.
[16] L.M. Molina, B. Hammer, Active role of oxide support during CO oxidation at Au/MgO, Phys. Rev. Lett. 90 (2003) 206102–206104.
[17] M.M. Schubert, S. Hackenberg, A.C. van Veen, M. Muhler, V. Plzak, R.J. Behm, CO oxidation over supported gold Catalysts—"Inert" and "active" support materials and their role for the oxygen supply during reaction, J. Catal. 197 (2001) 113.
[18] N. Qiao, J. Zheng, Nonenzymatic glucose sensor based on glassy carbon electrode modified with a nanocomposite composed of nickel hydroxide and graphene, microchim, Acta 177 (2012) 103–109.
[19] B. Zhan, C. Liu, H. Chen, H. Shi, L. Wang, P. Chen, W. Huang, X. Dong, Free-standing electrochemical electrode based on $Ni(OH)_2$/3D graphene foam for nonenzymatic glucose detection, Nanoscale 6 (2014) 7424.
[20] E.G.C. Neiva, M.M. Oliveira, M.F. Bergamini, L.H. Marcolino, A.G.H. Zarbin, One material, multiple functions: graphene/$Ni(OH)_2$ thin films applied in batteries, electrochromism and sensors, sci, For. Rep. 6 (2016) 33806.
[21] M.A. Kiani, M.A. Tehrani, H. Sayahi, Reusable, Robust High, Sensitive non-enzymatic glucose sensor based on $Ni(OH)_2$ nanoparticles, Anal. Chim. Acta 839 (2014) 26–33.
[22] E.W. Nery, M. Kundys, P.S. Jelen, M. Jönsson-Niedziółka, Electrochemical glucose sensing: is there still room for improvement, Anal. Chem. 88 (2016) 11271–11282.
[23] M. Waqas, L. Wu, H. Tang, C. Liu, Y. Fan, Z. Jiang, X. Wang, J. Zhong, W. Chen, Cu_2O microspheres supported on sulfur-doped carbon nanotubes for glucose sensing, ACS Appl. Nano Mater. 3 (2020) 4788–4798.
[24] A.K. Locke, A.K. Means, P. Dong, T.J. Nichols, L. Coté, Gerard, M.A. Grunlan, A layer-by-layer approach to retain a fluorescent glucose sensing assay within the cavity of a hydrogel membrane,, ACS AuthorChoice 1 (2018) 1319–1327.
[25] J. Li, H. Wu, I. Santana, Mackenzie Fahlgren, J. Giraldo, Standoff optical glucose sensing in photosynthetic organisms by a quantum dot fluorescent probe, ACS Appl. Mater. Interfaces 10 (2018) 28279–28289.
[26] R. Ballerstadt, J.S. Schultz, A fluorescence affinity hollow fiber sensor for continuous transdermal glucose monitoring,, Anal. Chem. 72 (2000) 4185–4192.
[27] M. Wang, X. Song, B. Song, J. Liu, C. Hu, D. Wei, C.P. Wong, Precisely quantified catalyst based on in situ growth of Cu_2O nanoparticles on a graphene 3D network for highly sensitive glucose sensor, Sens. Actuators, B 250 (2017) 333–341.
[28] C.M. Zhang, Z.W. Zhang, Q. Yang, W. Chen, Graphenebased electrochemical glucose sensors: Fabrication and sensing properties, Electroanalysis 30 (2018) 2504–2524.
[29] P.R. Solanki, A. Kaushik, V.V. Agrawal, B.D. Malhotra, Nanostructured metal oxide-based biosensors, NPG Asia Mater. 3 (2011) 17–24.
[30] N.J. Ronkainen, H.B. Halsall, W.R. Heineman, Electrochemical biosensors, Chem. Soc. Rev. 39 (2010) 1747–1763.
[31] C. Guo, H. Huo, X. Han, C. Xu, H. Li, Ni/CdS bifunctional Ti@TiO_2 core-shell nanowire electrode for high-performance nonenzymatic glucose sensing, Anal. Chem. 86 (2014) 876–883.
[32] Q. Li, P. Xu, B. Zhang, H. Tsai, S.J. Zheng, G. Wu, H.-L. Wang, Structure-dependent electrocatalytic properties of Cu_2O nanocrystals for oxygen reduction reaction, J. Phys. Chem. C 117 (2013) 13872–13878.
[33] X. Kang, J. Wang, H. Wu, I.A. Aksay, J. Liu, Y. Lin, Glucose oxidase-graphene-chitosan modified electrode for direct electrochemistry and glucose sensing, Biosens. Bioelectron. 25 (2009) 901–905.
[34] X. Zhang, G. Wang, X. Liu, J. Wu, M. Li, J. Gu, H. Liu, B. Fang, Different CuO nanostructures: synthesis, characterization, and applications for glucose sensors, J. Phys. Chem. C 112 (2008) 16845–16849.